Identification of the arrhythmogenic substrate in Brugada Syndrome: a computational study

Paolo Seghetti[1,2], Niccolò Biasi[3], Matteo Mercati[3], Valentina Hartwig[2], Andrea Rossi[2], Marco Laurino[2], Alessandro Tognetti[3,4]

1 Health Science Interdisciplinary Center, Scuola Superiore Sant'Anna, Pisa, Italy
2 Institute of Clinical Physiology, National Research Council, Pisa, Italy
3 Information Engineering Department, University of Pisa, Pisa, Italy
4 Research Centre "E. Piaggio", University of Pisa, Pisa, Italy
`paolo.seghetti@santannapisa.it`,

Abstract. Brugada syndrome (BrS) is a primarily electrical epicardial disease that increases the risk of sudden cardiac death. Arrhythmic events in BrS originate from the BrS substrate, located in the right ventricular outflow tract. Risk stratification in BrS patients is still controversial, with several models that have been recently proposed, especially for asymptomatic patients. In this contribution, we developed a computational model of the human right ventricle with alterations that represent the BrS substrate. The model is used to study the arrhythmogenic mechanism of BrS and the effect of different electrophysiological alterations on simulated epicardial unipolar electrograms (UEGs). We observed that the presence of diffuse fibrosis and repolarization abnormalities creates reentrant circuits that induce ventricular arrhythmia. Additionally, we found that repolarization and depolarization abnormalities have a similar effect on simulated UEGs, resulting in J/ST elevation. Our results link features observed on UEGs to the electrophysiological condition of the BrS substrate, offering new information that could be useful in risk stratification of BrS patients.

Keywords: Brugada Syndrome, Computational Simulation, Bioengineering

1 Introduction

Brugada Syndrome (BrS) is a primary electrical epicardial disease characterized by ST-segment elevation in the right precordial leads on the surface electrocardiogram (ECG) and by an increased risk of sudden cardiac death (SCD) due to polymorphic ventricular arrhythmias. The diagnostic type-1 BrS ECG pattern is characterized by ST elevation and negative T wave in the precordial leads (V1-V2), whereas two other patterns (type 2 and 3) have more subtle alterations in the J wave but are not diagnostic unless converted into a type 1 upon pharmacological challenge [1]. The electroanatomical substrate of BrS, mostly located in the epicardial layer of the right ventricular outflow tract (RVOT), typically

exhibits low voltage and fractionated local electrograms. BrS patients with previous cardiac arrest due to ventricular tachycardia/fibrillation (VT/VF) or syncope, in combination with spontaneous type-1 electrocardiographic phenotype, are recommended to implant a cardiac defibrillator (ICD) due to a high risk of arrhythmic prognosis. On the other hand, indications for a prophylactic ICD implantation are still debated in BrS patients. Several statistical models combining clinical factors and inducibility of ventricular arrhythmias at the electrophysiological study (EPS) have been proposed to improve prognostic stratification in BrS patients, but have been proved not specific enough to be used as indicators of VF [2]. Currently, two major hypotheses are considered for the pathological mechanism of BrS, the repolarization hypothesis and the depolarization hypothesis. The repolarization hypothesis proposes that an outward shift in the balance of membrane currents (sodium, calcium, or potassium) during phase 0-1 of the action potential (AP) leads to repolarization abnormalities in the tissue (i.e., loss of action potential dome), which in turn causes phase 2 reentry (P2R) and ectopic beats precipitating VF. Since the RVOT presents a higher expression of transient outward potassium channels, the current imbalance is higher in this region of the heart and thus the localization of the BrS substrate [3].

The depolarization hypothesis proposes that structural factors in the Right Ventricular (RV) epicardium (e.g., localized diffuse fibrosis) slow down the ventricular conduction and cause fractionated EGMs typically observed in the BrS substrate. This phenomenon is exacerbated in presence of sodium or calcium channel blockers, or potassium agonists, leading to local excitation failure [4, 5].

In this contribution, we present a computational model of a human RV with alterations that capture the salient features of the BrS substrate. The model is used to study the arrhythmogenic mechanism in BrS and to highlight how electrophysiological and structural alterations affect the morphology of epicardial Unipolar Electrograms (UEGs). To simulate healthy myocardial tissue, we used our previously developed myocyte phenomenological model fitted to healthy myocardial data [6]. To simulate BrS conditions, we introduced electrophysiological and structural abnormalities in the region corresponding to the epicardium of the RVOT by modifying the myocyte model parameters and introducing diffuse fibrosis. We obtained the parameters of the myocyte model in the BrS region by reproducing the AP morphology of epicardial monophasic action potentials recorded in vivo in humans [7]. In addition to studying the arrhythmogenic substrate, we performed 2 additional sets of simulations to assess the effect of either repolarization abnormalities or depolarization abnormalities on UEGs. This was done to study the effect of alterations in repolarization or depolarization on the morphology of UEGs, since both may be present in the BrS substrate [4]. The aim of this contribution is to elucidate the mechanisms behind arrhythmogenesis in BrS and to explore the basis for a model-based approach for prognostic stratification purposes by using patient-specific electrograms.

2   Methods

2.1   Myocyte model

We employed our previously published myocyte model to simulate BrS myocytes and healthy cardiac epicardial and endocardial tissue [6, 8, 9]. We defined the parameters of the BrS myocyte model to reproduce the AP characteristics commonly observed in humans [7] such as slow upstroke velocity and prominent AP notch. To reproduce the prominent AP notch, commonly linked to a transient outward current (I_{TO}) shift, we acted on the parameter d_w^0. Low values of d_w^0 increase I_{TO} and cause the prominent notch observed in BrS APs. Further reduction of d_w^0 induces complete loss of AP dome due to the fast repolarization of the membrane below the activation threshold. In the set of simulations aimed to determine the effect of depolarization abnormalities on UEGs, we modified parameters associated with a reduction in the depolarizing current of the myocyte. To reduce the upstroke velocity, commonly associated with mutations that reduce sodium current, we applied reduced values of the parameters γ_0 and γ_1. We also investigated the effect of AP amplitude and plateau voltage on the simulated UEG. To reduce the peak voltage during phase 1 of the AP, we reduced $A0$, and to reduce the plateau voltage we reduced $A1$.

2.2   Numerical methods

To simulate AP propagation, we incorporated the myocyte model in the monodomain formulation of the heart tissue. Due to the specific location of the BrS substrate in the RVOT, we simulated the AP propagation on a human RV and included electrophysiological and structural alterations in the epicardial RVOT (*BrS region*). In the BrS region we employed the BrS myocyte model, while in the remaining part of the RV we employed the healthy myocyte model adapted to endocardial and epicardial tissues. Moreover, to replicate the higher amount of fibrosis in the RVOT of BrS patients when compared with controls [5], we introduced diffuse fibrosis in the BrS region. Fibrosis was modeled as inexcitable obstacles of dimension 1×1 dx, and 50 % of tissue was replaced randomly by fibrosis.

Spatial derivatives were approximated with a second order central finite difference scheme ($dx = 0.15$ mm), temporal integration was carried out using the Euler method ($dt = 0.1$ $msec$). To implement no flux boundary conditions, we used the phase field method proposed by Fenton et al. [11]. We solved the monodomain equation only for points with a phase field value $> 1e - 4$, as suggested in the original article. Fibers orientation for points whose phase field value is above the aforementioned threshold but outside the initial geometry was interpolated with the nearest neighbor approach.
The RV realistic geometry was taken from the Zenodo open repository [10] (geometry N° 23) and extracted using Paraview. The geometries are available as meshes, so we resampled and interpolated them into a structured, homogeneous

voxel grid of $dx = 0.15\ mm$ by using default filters in Paraview. The transmural coordinate provided within the mesh was used to distinguish between the epicardial and endocardial layer, coordinates from 0 to 0.63 were considered endocardial, the remaining were considered epicardial. Orientation of the cardiac fibers was provided within the geometry and interpolated to the desired resolution, the anisotropy ratio was set to 1:4.

To reproduce the activation pattern in the RV, we used the method proposed by Ulysses et al. [12]. The method, while simple, allows the computation of approximate activation times without knowledge of locations of the Purkinje Muscle Junctions (PMJs), which is the case for the considered geometry. Cardiac tissue was activated from the endocardial layer, by injecting a current equal to twice the diastolic threshold into the myocytes at PMJs locations. In each simulation, cardiac tissue was initialized at the resting state (i.e., $Vm = -85mv; u = 0; w = 0$), then the tissue was stimulated by the PMJs at the computed activation times, with a period of 800 $msec$. The results presented in this work are taken from the last activation cycle simulated ($t > 3200\ msec$).

In addition, we simulated UEGs taken from an electrode placed on the epicardial surface of the RVOT. We computed UEGs using the homogeneous isotropic conductor theory. Figures of the heart were rendered using VOXview [13].

2.3   Simulations

To study the arrhythmogenic mechanism of BrS, we performed 3 simulations to replicate the following conditions: 1) healthy RV; 2) electrophysiological alterations in the BrS region without fibrosis; 3) electrophysiological alterations in the BrS region with fibrosis. In the second and third simulations, we introduced the same level of electrophysiological alterations ($d_w^0 = 0.3;\ \gamma_0 = 3;\ \gamma_1 = 7$).

Finally, to assess the effect of delayed depolarization vs early repolarization on the morphology of UEGs, we introduced changes in the electrophysiological behavior of the RVOT in 2 different sets of simulations. In the delayed depolarization set, we reduced the upstroke velocity and amplitude of the AP dome (by varying $A0;\ A1;\ \gamma_0;\ \gamma_1$), while in the early repolarization set of simulations we reduced upstroke velocity and increased the transient outward current (by varying $d_w^0;\ \gamma_0;\ \gamma_1$), as we did for the BrS case.

3   Results

3.1   Mechanism of arrhythmogenesis

In the healthy case (Fig. 1A), depolarization was homogeneous in the whole RV, starting from the PMJs in the endocardial layer and propagating toward the epicardium, from apex to base. Depolarization of the whole RV lasted $\simeq 80\ msec$. Repolarization started in the earliest activated regions (i.e., RV apex) and ended in the latest activated regions (i.e., RV base and RVOT). In presence of electrophysiological alterations and without fibrosis (Fig. 1B), depolarization in the

RVOT was not significantly slower. Additionally, repolarization in the RVOT occurred early due to the loss of AP dome, leaving a large repolarized region (refer to Fig. 1B when $t = 3500 \ ms$). In presence of electrophysiological alterations and fibrosis (Fig. 1C), depolarization during the first simulated beat was similar to the other 2 cases, then reentrant circuits caused tachycardia before the second beat occurred. Notably, the RV repolarization pattern in presence of electrophysiological alterations, with or without fibrosis, was similar. However, the presence of fibrosis caused the formation of reentrant circuits in the repolarized region (refer to Fig.1C). In the cases presented in Fig.1B and Fig.1C, the strong I_{TO} shift in the BrS region causes epicardial APs devoid of a dome. Without fibrosis, lost dome APs do not cause reentry in the healthy tissue and vanish as repolarization starts in the whole RV. The presence of fibrosis causes fragmentation of the AP wavefront, which can break and cause separate spiraling reentrant circuits, that excite again the healthy tissue after the refractory period, in accordance with the percolation theory [14].

3.2   UEGs

We performed 6 simulations to assess the effect of delayed depolarization vs early repolarization on the morphology of UEGs acquired from an electrode placed on the epicardial surface of the RVOT (position shown by the black circle in Fig.1). A first set of 3 simulations was used to assess the effect of I_{TO} shift on the UEGs (Fig. 2A). A second set of 3 simulations was used to assess the effect of reduced upstroke velocity and amplitude of the AP dome (Fig. 2B). In the first rows of Fig. 2A and Fig. 2B we report epicardial UEGs computed in the simulations. The second rows show the membrane potential of the epicardial (magenta) and endocardial (cyan) myocytes at the electrode position. In Fig.2A, as I_{TO} increases, UEGs transition from relatively normal ($\gamma_0 = 3.5; \ \gamma_1 = 7; \ d_w^0 = 0.5$, only J wave elevation) to prominent J/ST elevation ($\gamma_0 = 3.5; \ \gamma_1 = 7; \ d_w^0 = 0.4$) and UEGs with almost only positive components, called monophasic ($\gamma_0 = 3.5; \ \gamma_1 = 7; \ d_w^0 = 0.3$). Similarly, in Fig.2B, as the upstroke velocity and amplitude of the AP dome are reduced, UEGs transition from relatively normal (left, no changes in upstroke ($\gamma_0 = 3.5; \ \gamma_1 = 7;$) or AP dome($A0 = 90; \ A1 = 500;$)) to prominent J/ST elevation (middle, reduced upstroke velocity ($\gamma_0 = 1; \ \gamma_1 = 3;$) and AP dome ($A0 = 50; \ A1 = 500;$)) and monophasic UEG (right, reduced upstroke velocity ($\gamma_0 = 1; \ \gamma_1 = 3;$) and AP dome ($A0 = 50; \ A1 = 100;$)).

The first noticeable difference between the two sets of simulations is that the complete loss of AP dome causes a wider J/ST elevation than just the reduction of AP and upstroke velocity. Furthermore, the loss of AP dome causes additional deflections after the first depolarization, which are not present if AP dome is not completely lost, as in the case of Fig.2B.

4   Discussion

Our whole ventricle results show an arrhythmogenic mechanism that is compatible with the current clinical findings on BrS patients [5]. According to our model, arrhythmic events would occur when a patient's substrate precipitates from a condition of low electrophysiological alteration to a condition where lost dome APs appear in the substrate and wave break occurs because of fibrosis.

Our simulated UEGs have a morphology similar to those observed in BrS patients. Furthermore, J/ST elevation in simulated UEGs increases with electrophysiological alterations, as observed in BrS patients' UEGs [5]. For each set of substrate conditions, we can identify three different levels of J/ST elevation, similar to those observed in BrS patients [15].

The main difference between our simulated UEGs and experimental ones is in the T wave. In our model, T waves are not as prominent as the ones measured in patients' UEGs. Another difference is in the number of deflections observed when I_{TO} is strong. In the case report we considered [15], only one deflection seems to appear in the region with the highest electrophysiological alteration, however, we can not rule out that additional deflections can not be observed in BrS patients, maybe due to low membrane potential. Notably, in our model, deflections in UEGs are caused by the propagation of reentrant waves in the BrS substrate, as observed in animal models [3].

5   Conclusion

By defining an arrhythmogenic mechanism for BrS in a simulated RV, we are able to link the condition of the simulated BrS substrate to features in UEGs simulated in the BrS region. This could help to determine the condition of the BrS substrate from electroanatomical mapping on BrS patients. By the proposed arrhythmogenic mechanism, patients with higher J/ST elevation in UEGs would be at higher risk, since, according to our model, these are caused by lost dome waves, which generate reentrant circuits. However, as shown in Fig.2, similar UEG morphologies could be caused by different substrates, so future work is needed to find a reliable criterion to distinguish between J/ST elevation caused by delayed upstroke and reduced dome versus a loss of AP dome.
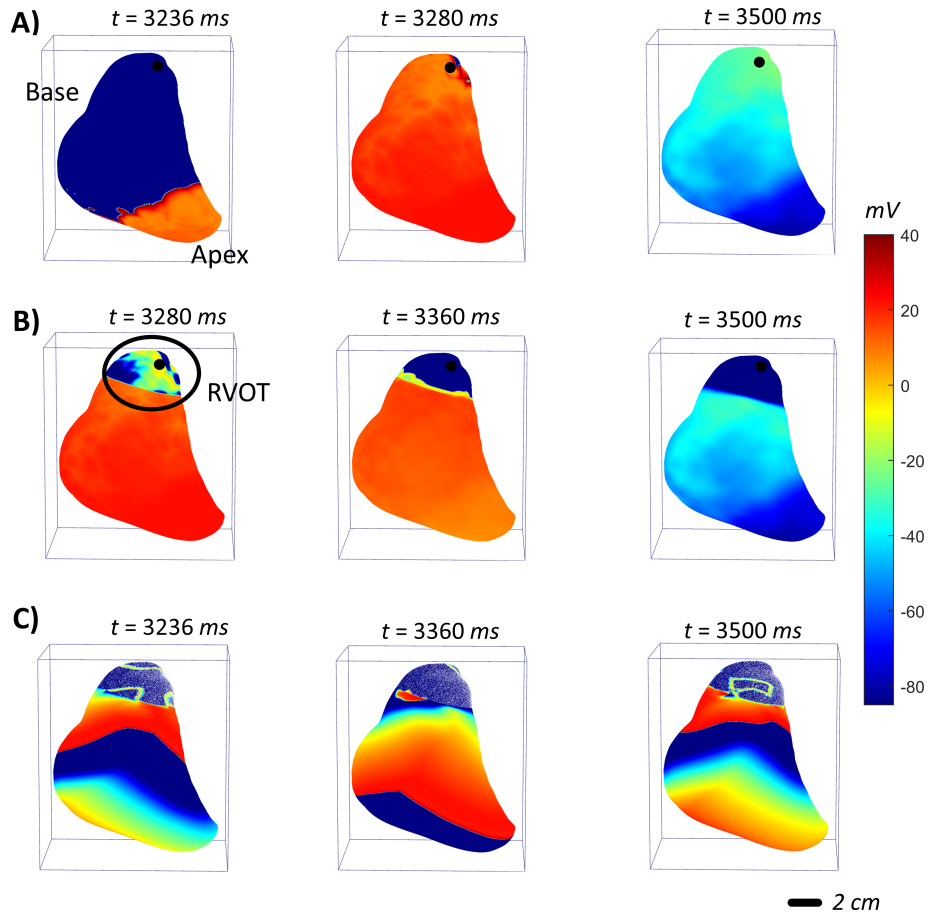
Acknowledgments

Fig. 1. Activation sequence of the RV for the 3 simulated scenarios. A: healthy; depolarization starts from the apex and ends in the base. Likewise, repolarization starts from the apex and ends in the RV base. B: repolarization abnormalities $d_w^0 = 0.3$, without fibrosis; depolarization is similar to the healthy case, three short APs are elicited in the RVOT, then the region remains unexcited until total repolarization. C: repolarization abnormalities $d_w^0 = 0.3$, with 50% of fibrosis; tachycardia is initiated by reentrant circuits in the RVOT .
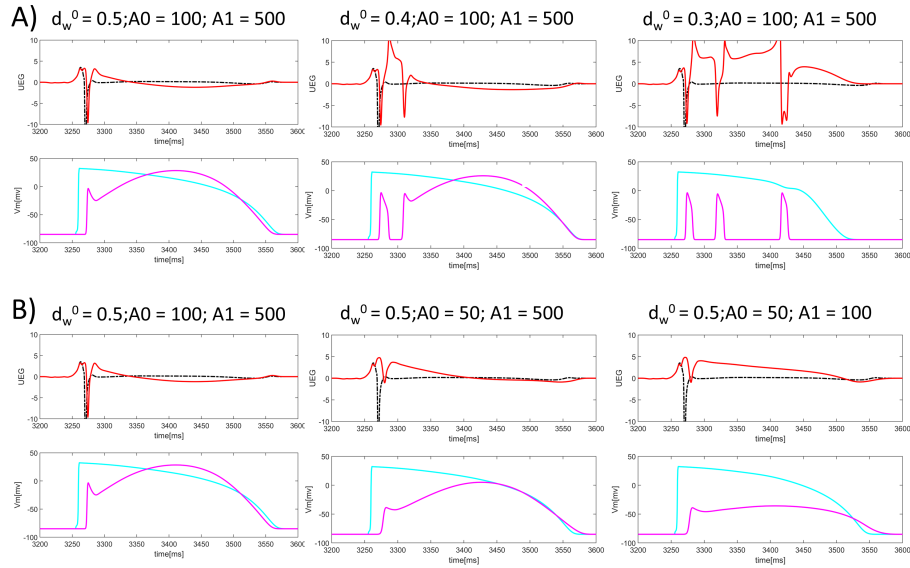
Fig. 2. Epicardial Unipolar Electrograms (UEGs) acquired over the BrS region at different levels of electrophysiological alterations, from left to right alterations are increased (top row). The dashed black line shows a healthy UEG simulated in the same location, the red line shows the UEG computed for the set of parameters. The bottom rows show epicardial (magenta) and endocardial (cyan) APs at the nearest location with respect to the electrode position. Parameters adopted in the respective simulations are reported on top of each panel. A: different UEG morphologies caused by I_{TO} shift in the epicardial layer of the RVOT. Additional deflections in the UEGs are caused by reentrant beats in the epicardial layer of the RVOT, but do not elicit a reentry in the healthy tissue. B: different UEG morphologies caused by reduced upstroke velocity and dome amplitude in the epicardial layer of the RVOT, a single deflection is observed. Note that J/ST elevation has a lower amplitude when compared to the other set of simulations.

References

1. Delise, P., Probst, V., Allocca, G., Sitta, N., Sciarra, L., Brugada, J., Kamakura, S., Takagi, M., Giustetto, C. & Calo, L. Clinical outcome of patients with the Brugada type 1 electrocardiogram without prophylactic implantable cardioverter defibrillator in primary prevention: a cumulative analysis of seven large prospective studies. *EP Europace.* **20**, f77-f85 (2018)
2. Letsas, K., Asvestas, D., Baranchuk, A., Liu, T., Georgopoulos, S., Efremidis, M., Korantzopoulos, P., Bazoukis, G., Tse, G., Sideris, A. & Others Prognosis, risk stratification, and management of asymptomatic individuals with Brugada syndrome: a systematic review. *Pacing And Clinical Electrophysiology.* **40**, 1332-1345 (2017)
3. Antzelevitch, C. & Di Diego, J. J wave syndromes: What's new?. *Trends In Cardiovascular Medicine.* **32**, 350-363 (2022)
4. Weiss, J. Arrhythmias in Brugada syndrome: defective depolarization, repolarization or both?. *Clinical Electrophysiology.* **7** pp. 271-272 (2021)
5. Nademanee, K., Veerakul, G., Nogami, A., Lou, Q., Hocini, M., Coronel, R., Behr, E., Wilde, A., Boukens, B. & Haissaguerre, M. Mechanism of the effects of sodium channel blockade on the arrhythmogenic substrate of Brugada syndrome. *Heart Rhythm.* **19**, 407-416 (2022)
6. Biasi, N., Seghetti, P. & Tognetti, A. A transmurally heterogeneous model of the ventricular tissue and its application for simulation of Brugada Syndrome. *2022 44th Annual International Conference Of The IEEE Engineering In Medicine & Biology Society (EMBC).* pp. 3951-3954 (2022)
7. Kurita, T., Shimizu, W., Inagaki, M., Suyama, K., Taguchi, A., Satomi, K., Aihara, N., Kamakura, S., Kobayashi, J. & Kosakai, Y. The electrophysiologic mechanism of ST-segment elevation in Brugada syndrome. *Journal Of The American College Of Cardiology.* **40**, 330-334 (2002)
8. Biasi, N., Seghetti, P. & Tognetti, A. Diffuse fibrosis and repolarization disorders explain ventricular arrhythmias in Brugada syndrome: a computational study. *Scientific Reports.* **12**, 8530 (2022)
9. Biasi, N. & Tognetti, A. A computationally efficient dynamic model of human epicardial tissue. *Plos One.* **16**, e0259066 (2021)
10. Strocchi, M., Augustin, C., Gsell, M., Karabelas, E., Neic, A., Gillette, K., Razeghi, O., Prassl, A., Vigmond, E., Behar, J. & Others A publicly available virtual cohort of four-chamber heart meshes for cardiac electro-mechanics simulations. *PloS One.* **15**, e0235145 (2020)
11. Fenton, F., Cherry, E., Karma, A. & Rappel, W. Modeling wave propagation in realistic heart geometries using the phase-field method. *Chaos: An Interdisciplinary Journal Of Nonlinear Science.* **15**, 013502 (2005)
12. Ulysses, J., Berg, L., Cherry, E., Liu, B., Dos Santos, R., Barros, B., Rocha, B. & Queiroz, R. An optimization-based algorithm for the construction of cardiac purkinje network models. *IEEE Transactions On Biomedical Engineering.* **65**, 2760-2768 (2018)
13. VOXview (https://www.mathworks.com/matlabcentral/fileexchange/78745-voxview), MATLAB Central File Exchange. Retrieved March 8, 2023.
14. Alonso, S., Dos Santos, R. & Bär, M. Reentry and ectopic pacemakers emerge in a three-dimensional model for a slab of cardiac tissue with diffuse microfibrosis near the percolation threshold. *PloS One.* **11**, e0166972 (2016)
15. Kataoka, N., Nagase, S., Kamakura, T., Noda, T., Aiba, T. & Kusano, K. Local activation delay exacerbates local J-ST elevation in the epicardium: Electrophys-

iological substrate in Brugada syndrome. *HeartRhythm Case Reports.* **3**, 595-598 (2017)